

Quantum vortices leave a macroscopic signature in the normal fluid

Luca Galantucci,^{1,2,*} Giorgio Krstulovic,^{3,†} and Carlo F. Barenghi^{2,‡}

¹*Istituto per le Applicazioni del Calcolo M. Picone, IAC-CNR, Via dei Taurini 19, Roma 00185, Italy*

²*School of Mathematics, Statistics and Physics, Newcastle University, Newcastle upon Tyne NE1 7RU, United Kingdom*

³*Université Côte d'Azur, Observatoire de la Côte d'Azur, CNRS, Laboratoire*

J. L. Lagrange, Boulevard de l'Observatoire CS 34229 - F 06304 NICE Cedex 4, France

(Dated: January 15, 2025)

Recent work has highlighted the remarkable properties of quantum turbulence in superfluid helium II, consisting of a disordered tangle of quantised vortex lines which interact with each other and reconnect when they collide. According to Landau's two-fluid theory, these vortex lines move in a surrounding of thermal excitations called the *normal fluid*. Until now, the normal fluid has often been considered a passive background which simply provides the vortex lines with a mechanism for dissipating their kinetic energy into heat. Using a model which fully takes into account the two-way interaction between the vortex lines and the normal fluid, here we show that each vortex line creates a macroscopic wake in the normal fluid that can be larger than the average distance between vortex lines; this is surprising, given the microscopic size of the superfluid vortex cores which induce these wakes. We show that in heat transfer experiments, the flow of the normal fluid can therefore be described as the superposition of an imposed uniform flow and wakes generated by the vortex lines, leading to non-classical statistics of the normal fluid velocity. We also argue that this first evidence of independent fluid structures in the thermal excitations postulated by Landau may be at the root of recent, unaccounted for, experimental findings.

It was Landau who first understood that the properties of a many-body quantum system such as helium II depend on thermally excited elementary excitations - collective modes which he called phonons and rotons depending on whether their dispersion relation is linear or quadratic. This idea has influenced many areas of modern physics since. In the context of liquid helium, Landau's intuition led to the formulation of the two-fluid theory, which accounts for unusual behaviours of helium II, from second sound and thermal counterflows¹ to critical velocities². Briefly, helium II behaves as the mixture of two inseparable fluid components: the viscous normal fluid (associated to the thermal excitations) and the inviscid superfluid (associated to the ground state). Each component has its own density field and velocity field, ρ_s, \mathbf{v}_s for the superfluid and ρ_n, \mathbf{v}_n for the normal fluid, where $\rho = \rho_n + \rho_s$ is the total density. As a consequence, two distinct motions occur simultaneously at the same position in space. Of the two components, only the normal fluid has nonzero entropy (hence is capable of carrying heat). Because of quantum mechanical constraints, the superfluid's vorticity is concentrated to vortex lines of quantised circulation (in units of h/m where h is Planck's constant and m is the mass of one helium atom) and microscopic thickness (the vortex core radius is only $a_0 \approx 0.1$ nm). Over the years, the vortex lines have attracted great attention, revealing remarkable properties: vortex lattices³, vortex nucleation⁴, Kelvin waves^{5,6}, vortex reconnections⁷, and quantum turbulence⁸ of various kinds⁹.

In contrast, much less attention has been paid to the nor-

mal fluid, of which we still know very little. We know that Landau's excitations are scattered by the velocity field of the vortex lines, creating a mutual friction between the two fluid components which allows energy exchange^{10,11}. For the sake of simplicity, in most problems it is usually assumed that the normal fluid is spatially uniform or at rest, simply providing a dissipative background to the vortex lines.

Based on the mean free path λ and the Knudsen number λ/d , the description of Landau's excitations as a fluid (rather than a ballistic gas) is appropriate for lengthscales $d > 0.2 \mu\text{m}$ at $T = 1.5$ K and $d > 0.02 \mu\text{m}$ at $T = 2.1$ K, which is the temperature range of interest here. These values of d are safely smaller than both the size of tracer particles used to visualize flows ($\gtrsim 1 \mu\text{m}$)¹²⁻¹⁶ and the typical distance between vortex lines in turbulence experiments, $\ell \approx 10$ to $100 \mu\text{m}$. It is therefore natural to assume that the normal fluid obeys no-slip boundary conditions, but what should be the normal fluid's large-scale velocity profile in a channel is still an open question. For coflows (\mathbf{v}_s and \mathbf{v}_n flowing in the same direction, e.g. driven by bellows) a laminar normal fluid profile has been observed¹⁷ but its scaling with the Reynolds number has not been explained yet. For counterflows (\mathbf{v}_s and \mathbf{v}_n flowing in opposite direction driven by a heater) there is theoretical debate about the shape of the laminar profile^{18,19}, and experimental evidence (but no quantitative information) of a transition to turbulence at large velocity^{20,21}. Until now, no other flow structure, at any scale, has ever been identified in the normal fluid, which has remained somewhat mysterious.

The numerical results that we present here predict that the relative motion of vortex lines and the normal fluid creates, besides small dipolar structures²² which are probably too small to be observed, also large macroscopic wakes in

* luca.galantucci@cnr.it

† giorgio.krstulovic@oca.eu

‡ carlo.barenghi@newcastle.ac.uk

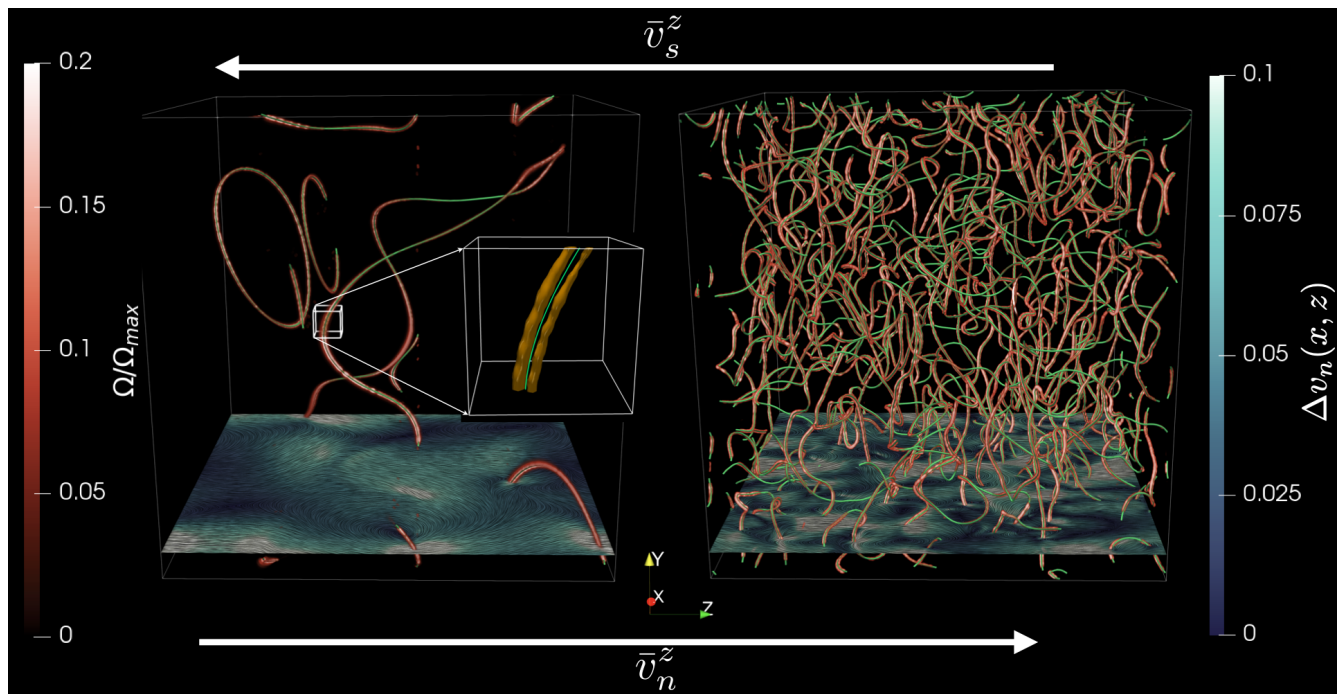


Fig. 1 Snapshots of vortex tangles. Turbulence at $T = 1.5$ K generated by counterflow velocities $v_{ns}^{(1)} = 0.27$ cm/s (left) and $v_{ns}^{(2)} = 0.94$ cm/s (right). The superfluid vortex lines are displayed as green curves and the normal fluid dipoles are visualized by the normalised enstrophy $\Omega(\mathbf{x})/\Omega_{max}$ in reddish color. The relative magnitude of normal fluid fluctuations $\Delta v_n(x, z)$ is plotted on a xz plane at constant y .

the normal fluid. The wakes are so large (even larger than the typical inter-vortex distance ℓ) that we predict they affect the velocity statistics of the normal fluid, producing skewed distributions with wide tails, strikingly dissimilar from classical turbulence. We shall see that some indirect evidence of this effect has been measured in counterflow turbulence experiments without being recognized.

Our numerical simulations of counterflow turbulence use the code FOUCAULT²³. The code models vortex lines as space-curves of infinitesimal thickness, which is appropriate given the huge separation of scales between the vortex core thickness a_0 and the typical distance ℓ between vortex lines in quantum turbulent flows. Unlike the original one-way approach of Schwarz²⁴, FOUCAULT accounts for the two-way interaction between the vortex lines (which evolve according to the Biot-Savart law and mutual friction corrections) and the normal fluid (which evolves according to a modified Navier-Stokes equation); as in the approach of Schwarz, vortex reconnections are implemented algorithmically. For simplicity our calculations are performed in a cube of size $D = 0.1$ cm with periodic boundary conditions (see Methods for details).

To model thermal counterflow, we impose average normal fluid and superfluid velocities along the positive and negative z -directions, respectively. This creates a counterflow velocity $v_{ns} = |\bar{v}_n^z - \bar{v}_s^z|$ (where overbars denote spatial averages) which, in the experiments, is proportional to the applied heat flux. The two fluid components flow in opposite directions: the normal fluid carries the

heat away from the heater at speed $\bar{v}_n^z = (\rho_s/\rho)v_{ns}$, while the superfluid flows in the opposite direction to conserve mass, $\bar{v}_s^z = -(\rho_n/\rho)v_{ns}$. The initial condition consists of few random vortex rings, which, after a transient, evolve into a statistically steady state, which is independent of the initial condition; at this point the vortex line density (defined as the length of vortex lines per unit volume) fluctuates around a mean value L corresponding to the average intervortex distance $\ell \approx 1/\sqrt{L}$. Our numerical experiments are performed at temperature $T = 1.5$ K at two distinct values of the counterflow velocity: $v_{ns}^{(1)} = 0.27$ cm/s and $v_{ns}^{(2)} = 0.94$ cm/s, yielding $L^{(1)} = 7.2 \times 10^2$ cm⁻² and $L^{(2)} = 1.1 \times 10^4$ cm⁻² respectively. These turbulent vortex tangles are anisotropic, as vortices tend to lie on xy planes perpendicular to the applied counterflow in the z direction.

Figure 1 shows snapshots of the computed vortex tangles corresponding to $v_{ns} = v_{ns}^{(1)}$ (left) and $v_{ns} = v_{ns}^{(2)}$ (right). The superfluid vortices are displayed as green curves, and the enstrophy of the normal fluid, defined as $\Omega(\mathbf{x}) = |\boldsymbol{\omega}_n(\mathbf{x})|^2/2$ (where $\boldsymbol{\omega}_n = \nabla \times \mathbf{v}_n$) and normalised by its maximum value Ω_{max} , is rendered in reddish colours according to the colormap reported on the left. At the bottom of each panel, we report a two-dimensional slice on a plane at fixed $y = y_0$ of the relative magnitude of in-plane normal fluid fluctuations $\Delta v_n(x, z) = \|\delta \tilde{\mathbf{v}}_n(x, y_0, z)\|/|\bar{v}_n^z|$, with $\delta \tilde{\mathbf{v}}_n = (v_n^x, v_n^z - \bar{v}_n^z)$, colour-coded by the colormap on the right.

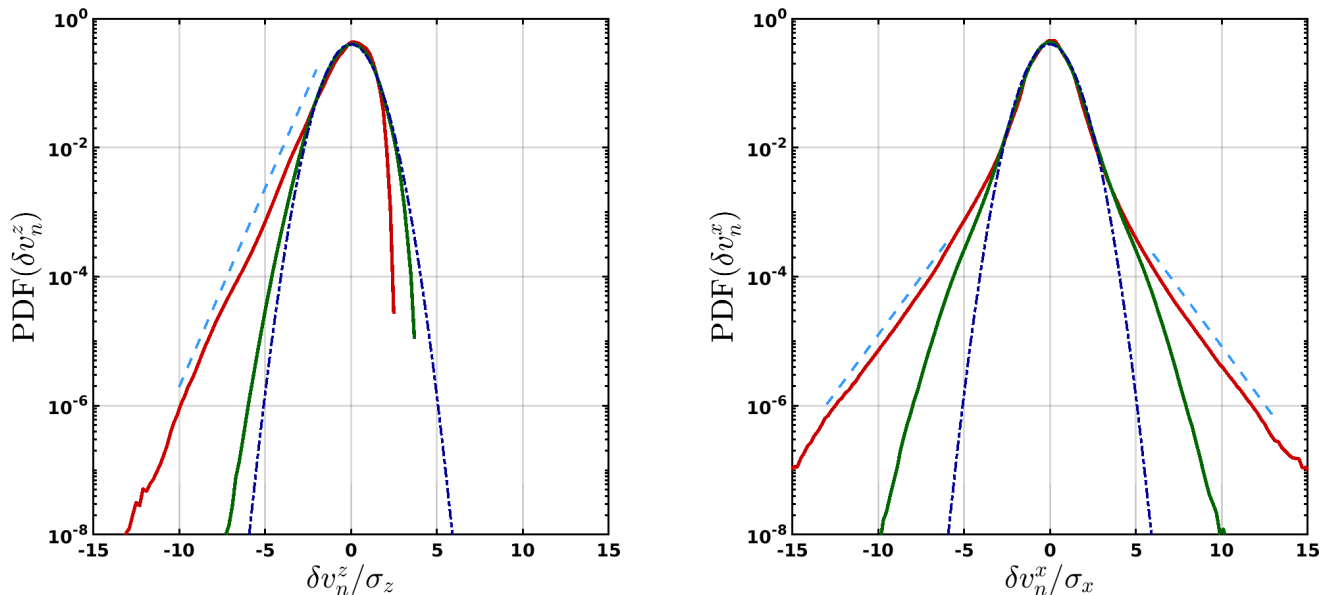


Fig. 2 PDFs of velocity fluctuations. Calculations at $T = 1.5$ K at the same parameters as Fig. 1. Left: streamwise PDF(δv_n^z) vs $\delta v_n^z/\sigma_z$ where σ_z is the standard deviation. Right: spanwise PDF(δv_n^x) vs $\delta v_n^x/\sigma_x$ where σ_x is the standard deviation. Red curves refer to $v_{ns}^{(1)} = 0.27$ cm/s and green curves to $v_{ns}^{(2)} = 0.94$ cm/s. Gaussian distributions are showed in dot-dashed dark blue line for reference. Dashed cyan curves are exponential fits to the wide tails.

Previous calculations^{22,25,26} have shown that each superfluid vortex is surrounded by two localised regions of large normal fluid enstrophy, essentially a vorticity dipole induced by the friction. This dipole is small, of the order of only few micrometers (≈ 2 to $4 \mu\text{m}$ ²⁵). The novel effect which here we report is the existence of much larger normal fluid structures, whose existence has been to some extent speculated²⁷, but not clearly observed. The two-dimensional slices for both low (left) and high (right) counterflow velocity regimes reported in Fig. 1, clearly show that in the proximity of superfluid vortices there are regions (almost two orders of magnitude larger than the dipoles) where \mathbf{v}_n is significantly different than $\bar{\mathbf{v}}_n$ (the magnitude of the normal fluid velocity fluctuations being up to 10% the applied normal fluid velocity \bar{v}_n^z). This is the first clear evidence of large scale (potentially observable experimentally) fluid structures which spontaneously appear in Landau's sea of thermal excitations.

Such large scale structures strongly modify and impact the statistical distribution of the normal fluid velocity. We concentrate the attention on the streamwise and spanwise velocity fluctuations, defined as $\delta v_n^z = v_n^z - \bar{v}_n^z$ and $\delta v_n^x = v_n^x$ (since $\bar{v}_n^x = 0$), respectively. In Fig. 2 we plot the probability distribution functions (PDFs) of the velocity fluctuations normalised by their respective variances σ_z and σ_x , for both counterflow values. $v_{ns}^{(1)} = 0.27$ cm/s (red) and $v_{ns}^{(2)} = 0.94$ cm/s (green), where σ_z and σ_x are the standard deviations of streamwise and spanwise velocities respectively.

The main result, shown in the left panel of Fig. 2, is that the PDFs of the streamwise velocity fluctuations are left-skewed, showing the predominance of negative

fluctuations. In other words there are large regions where the normal fluid flows slower than the average flow in the direction parallel to the applied counterflow. In the spanwise direction, on the contrary, the PDFs are symmetrical - see the right panel of Fig. 2. This effect is independent of the counterflow velocity; in the low counterflow case (red curves), we observe that the tails have an exponential behaviour.

Additionally, we find that, consistently with Particle Tracking Velocimetry (PTV) experiments at not too small counterflow velocities²⁸, the standard deviation of the streamwise velocity is larger than its spanwise counterpart: $\sigma_z \approx 2\sigma_x$. As we move from the low to high velocity regime, the tails and the skewness of the PDFs become less pronounced, while the standard deviations increase, again as observed experimentally²⁸. We conclude that the PDFs of the normal fluid in counterflow turbulence differ strikingly from the PDFs of velocity fluctuations in classical turbulence, which display a sub-Gaussian behaviour²⁹.

We argue that the low-velocity regions - the regions which we have identified in Fig. 1 - are wakes generated by the mutual friction force exerted by the vortex lines on the normal fluid. In fact, we find that the average speed of the vortex lines is about one tenth of \bar{v}_n^z for both $v_{ns}^{(1)}$ and $v_{ns}^{(2)}$. Essentially, vortices are like obstacles which slow down the normal fluid in the downstream region. As v_{ns} increases, the impact of these wakes on the PDFs is less pronounced (the PDFs tend to have a more Gaussian character) because wakes overlap, randomizing the flow.

In order to support our argument, we perform a numerical experiment in a simpler set-up, which clarifies the physics: a single, straight superfluid vortex oriented in

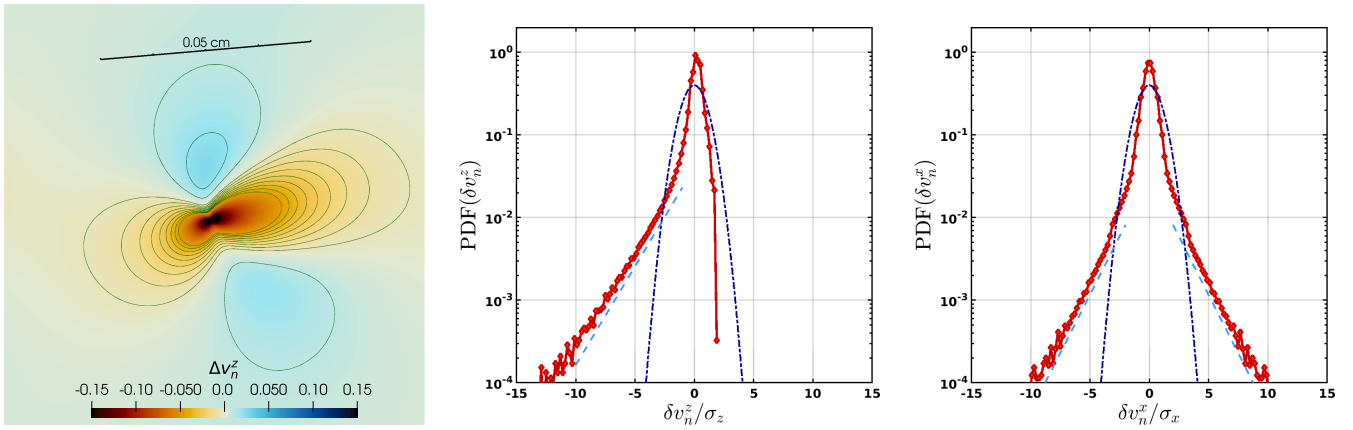


Fig. 3 Single vortex wake. Temperature $T = 1.5$ K and $v_{ns}^{(1)} = 0.27$ cm/s. Left column: relative normal fluid streamwise velocity fluctuations $\Delta v_n^z = \delta v_n^z / \bar{v}_n^z = (v_n^z(x, z) - \bar{v}_n^z) / \bar{v}_n^z$ vs x and z at fixed y_0 . The ruler indicates the direction of the relative velocity of the single vortex line with respect to the normal fluid. Centre column: PDF(δv_n^z) vs $\delta v_n^z / \sigma_z$, where $\delta v_n^z = v_n^z - \bar{v}_n^z$ and σ_z is the standard deviation. Right column: PDF(δv_n^x) vs $\delta v_n^x / \sigma_x$, where $\delta v_n^x = v_n^x$ ($\bar{v}_n^x = 0$) and σ_x is the standard deviation. Gaussian distributions are shown in dot-dashed dark blue line for reference. The dashed cyan lines are exponential functions to guide the eye.

the positive y -direction in the presence of counterflow in the z direction, at the same values of T and v_{ns} used for Fig. 1. We find that, after a short transient, the vortex moves at constant relative velocity with respect to the normal fluid. In a turbulent tangle, vortices move at a relatively constant velocity with respect to the normal fluid only for a fraction of the time between two successive reconnections τ_r , which can be estimated using the vortex line density L as $\tau_r \approx 6\pi / |\kappa L \ln(L^{1/2} a_0)|^{30}$. Consequently, we consider the pattern of the normal fluid past the single vortex at time $t \approx \tau_r / 10$. Fig. 3 displays the results of this numerical experiment using the counterflow velocity $v_{ns}^{(1)}$ (equivalent figures for $v_{ns}^{(2)}$ are provided in the Supplementary Information).

The left panel of Fig. 3, where contours lines are drawn at constant values of $(v_n^z(x, z) - \bar{v}_n^z) / \bar{v}_n^z$, shows that the normal fluid wake is almost parabolic. The size of the wake, computed as a velocity weighed distance from the vortex (see Supplementary Information), is $w^{(1)} = 190 \mu\text{m}$ for $v_{ns} = v_{ns}^{(1)}$ and $w^{(2)} = 140 \mu\text{m}$ for $v_{ns} = v_{ns}^{(2)}$, almost two orders of magnitude larger than the normal fluid vorticity dipoles²⁵. The misalignment of the direction of the relative velocity between the vortex and the normal fluid (indicated by the ruler in Fig. 3 (left)) and the axis of the wake arises from the Iordanskii force (see Methods). In the central and right panels of Fig. 3, we report the PDFs of the streamwise and spanwise normal fluid velocity fluctuations in our single vortex numerical experiment. We observe that the PDFs (centre and right panels) mimic the behaviour of the corresponding PDFs computed for the turbulent counterflow at the same counterflow velocity $v_{ns}^{(1)} = 0.27$ cm/s reported in Fig. 2 (red curves): skewed and/or with wide exponential tails.

The dipole and the parabolic wake induced by a vortex onto the normal fluid recall the classical Oseen solution of the slow viscous flow past a cylinder of ra-

dius a_0 equations³¹. Indeed, the assumptions behind the Oseen solution are well satisfied: the vortex is locally straight (its radius of curvature is $R_c \approx \ell \gg a_0$) hence the flow is two-dimensional, the Reynolds number $Re = \bar{v}_n^z a_0 / \nu_n$ (where ν_n is the kinematic viscosity) is very small: $Re^{(1)} = 0.3 \times 10^{-5}$ and $Re^{(2)} = 1 \times 10^{-5}$, and the scales at which we probe the flow are much larger than the cylinder's radius. Focusing on the far field solution at distances larger than the Oseen scale a_0 / Re , we recover both the vortex dipole and the parabolic wake in intensity and shape, and the skewed/exponential velocity fluctuation PDFs, as shown in Supplementary Information.

Our results thus suggest that the flow of the normal fluid in a turbulent helium counterflow can be described as the superposition of a uniform background flow generated by the heater and flow disturbances (consisting of small vortex dipoles and large almost parabolic wakes) generated by the vortices via the friction force. The less pronounced tails of the normal fluid velocity fluctuations for $v_{ns}^{(2)} = 0.94$ cm/s (Fig. 2, green curves) arise from the fact that the wake $w^{(2)}$ is larger than the average inter-vortex spacing $\ell^{(2)} = 94 \mu\text{m}$, hence wakes overlap randomising the flow. On the contrary, for $v_{ns}^{(1)} = 0.27$ cm/s, $w^{(1)} < \ell^{(1)} = 370 \mu\text{m}$, the wakes tend to be separated, and the velocity statistics of the normal fluid (Fig. 2, red curves) echo the case of an isolated vortex (Fig. 3, central and right panels).

The natural question is whether the normal fluid wakes that we predict can be detected in experiments. Non-destructive visualisation of the turbulent normal fluid has been achieved using metastable helium molecules²¹, but has not yet probed the length scales considered here. However, measurements obtained via the PTV visualization technique may show the signature of the wakes. Indeed, a recent PTV experiment at large counterflow velocities reported a left-skewed distribution for the streamwise

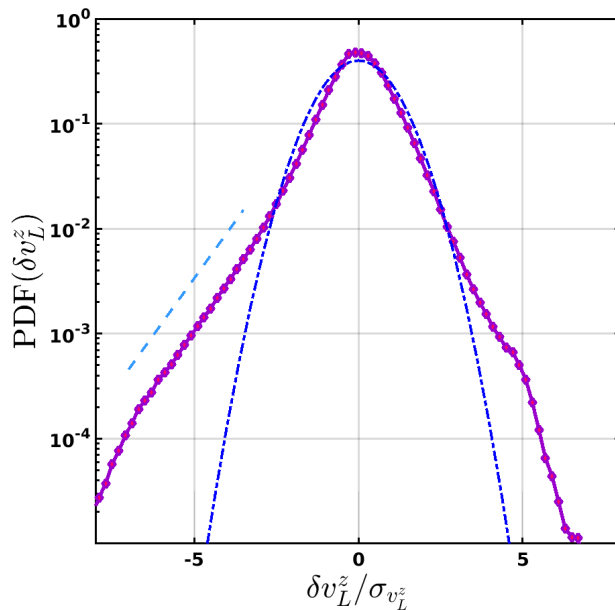


Fig. 4 Vortex statistics. Parameters: $T = 1.5$ K, $v_{ns} = v_{ns}^{(2)} = 0.94$ cm/s. Left: Distribution of the normal fluid's z -velocity component evaluated at the position of vortex lines, $\text{PDF}(v_n^z(\mathbf{s}))$ vs $v_n^z(\mathbf{s})$. The vertical red dashed line corresponds to \bar{v}_n^z . Right: Distribution of streamwise vortex velocity fluctuations $\text{PDF}(\delta v_L^z)$ vs $\delta v_L^z/\sigma_{v_L^z}$ where $\sigma_{v_L^z}$ is the standard deviation of v_L^z . The dot-dashed blue line is the Gaussian fit, and the cyan dashed line is a guide to the eyes to highlight the tail.

velocity of likely trapped particles (the so-called “slow” particles in Fig. 10 of Ref.³²), similar to the normal fluid streamwise velocity distributions that we calculate (our Fig. 2 (left)).

A similar left-skewed distribution (see Fig. 4) is recovered when calculating at $v_{ns} = v_{ns}^{(2)}$ (as experiments are performed at large v_{ns}) the distribution of the streamwise vortex velocity fluctuations $\delta v_L^z = v_L^z - \bar{v}_L^z$, where \mathbf{v}_L is the vortex velocity, confirming that the motion of particles trapped on vortices may be indeed approximated with the motion of the vortices themselves^{28,33}. It is possible to show (see Supplementary Information for details) that the skewness which characterises δv_n^z (Fig. 2 (left)) contributes to the enhance the skewness of δv_L^z (Fig. 4): the experimental signature of the normal fluid wakes is the left-skewed distribution of the streamwise velocity of likely trapped particles in PTV experiments³².

Finally, it is interesting to notice that the original one-way coupled theory of Schwarz²⁴ (where $\mathbf{v}_n = \bar{\mathbf{v}}_n$, prescribed *a priori*) predicts that, at $T = 1.5$ K, the vortex tangle drifts, with respect to the superfluid applied flow, at average velocity $\bar{v}_L^z - \bar{v}_s^z \approx 0.35v_{ns}$ in the direction of v_n^z ³⁴, as a result of the drag exerted by the normal fluid. A subsequent experiment³⁵ found that the average drift velocity of the vortices is smaller, reporting the upper limit $\bar{v}_L^z - \bar{v}_s^z < 0.2v_{ns}$ for this temperature. Our two-way coupled simulation finds $\bar{v}_L^z - \bar{v}_s^z \leq 0.15v_{ns}$, in good agreement with this experiment, showing indeed that vortices see a slower normal fluid as a result of the wakes.

In conclusion, our numerical experiments predict that counterflow turbulence can be described as the superposition of (i) the superflow and the normal flow (here

uniform) which are imposed by the heater, (ii) superfluid velocity fluctuations created by the turbulent vortex lines, and (iii) local perturbations of the normal fluid velocity induced by the friction. Two decades ago theory predicted²² that the vortex lines are surrounded by small dipolar vorticity structures in the normal fluid. The very small scale of these structures (comparable to the scale of the particles used for PTV visualization) has so far prevented any direct observation. The novel feature revealed by the work presented here is that, alongside the dipolar structures, the vortex lines also induce normal fluid wakes which can be larger than the average intervortex distance and affect the velocity statistics of the normal fluid, as the experiments that we have discussed suggest.

References

1. W. F. Vinen, Mutual friction in a heat current in liquid helium II. (iii) theory of mutual friction, Proc. R. Soc. London A **242**, 493 (1957).
2. S. Babuin, M. Stammeier, E. Varga, M. Rotter, and L. Skrbek, Quantum turbulence of bellows-driven 4He superflow: steady state, Phys. Rev. B **86**, 134515 (2012).
3. E. J. Yarmchuck, M. J. V. Gordon, and R. E. Packard, Observation of stationary vortex arrays in rotating superfluid helium through an aperture, Phys. Rev. Lett. **43**, 214 (1979).
4. O. Avenel and E. Varoquaux, Observation of singly quantized dissipation events obeying the josephson frequency relation in the critical flow of superfluid ⁴He through an aperture, Phys. Rev. Lett. **55**, 2704 (1985).
5. J. T. Mäkinen, S. Autti, P. J. Heikkinen, J. J. Hosio, R. Hänninen, V. S. L'vov, P. M. Walmsley, V. V. Zavjalov, and V. B. Eltsov, Rotating quantum wave turbulence, Nature Phys. **19**, 898 (2023).
6. C. Peretti, J. Vessaire, É. Durozoy, and M. Gibert, Direct visualization of the quantum vortex lattice structure, oscillations, and destabilization in rotating 4He, Sci. Adv. **9**, eadh2899 (2023).

7. E. Fonda, D. Meichle, B. Ouellette, S. Hormoz, and D. Lathrop, Direct observation of kelvin waves excited by quantized vortex reconnection, *Proc. Natl. Acad. Sci. USA* **111**, 4707 (2014).
8. L. Skrbek, D. Schmoranzner, S. Midlik, and K. R. Sreenivasan, Phenomenology of quantum turbulence in superfluid helium, *Proc. Natl. Acad. Sci. USA* **118**, e2018406118 (2021).
9. C. F. Barenghi, H. A. J. Middleton-Spencer, L. Galantucci, and N. G. Parker, Types of quantum turbulence, *AVS Quantum Science* **5**, 025601 (2023).
10. H. Hall and W. Vinen, The rotation of liquid helium II. i. experiments on the propagation of second sound in uniformly rotating helium ii, *Proc. R. Soc. London A* **238**, 204 (1956).
11. H. Hall and W. Vinen, The rotation of liquid helium II. ii. the theory of mutual friction in uniformly rotating helium ii, *Proc. R. Soc. London A* **238**, 215 (1956).
12. T. Zhang and S. W. Van Sciver, Large-scale turbulent flow around a cylinder in counterflow superfluid 4He (he II), *Nature Phys* **1**, 36 (2005).
13. G. P. Bewley, D. P. Lathrop, and K. P. Sreenivasan, Visualization of quantized vortices, *Nature* **441**, 588 (2006).
14. M. La Mantia, D. Duda, M. Rotter, and L. Skrbek, Lagrangian accelerations of particles in superfluid turbulence, *J. Fluid Mech.* **717**, R9 (2013).
15. Y. Tang, W. Guo, H. Kobayashi, S. Yui, M. Tsubota, and T. Kanai, Imaging quantized vortex rings in superfluid helium to evaluate quantum dissipation, *Nature Commun.* **14**, 2941 (2023).
16. W. Kubo and Y. Tsuji, Statistical properties of small particle trajectories in a fully developed turbulent state in he-ii, *J. Low Temp. Phys.* **196**, 170 (2019).
17. T. Xu and S. V. Van Sciver, Particle image velocimetry measurements of the velocity profile in he ii forced flow, *Phys. Fluids* **19**, 071703 (2007).
18. L. Galantucci, M. Sciacca, and C. Barenghi, Coupled normal fluid and superfluid profiles of turbulent helium ii in channels, *Phys. Rev. B* **92**, 174530 (2015).
19. S. Yui, M. Tsubota, and H. Kobayashi, Three-dimensional coupled dynamics of the two-fluid model in superfluid he 4: Deformed velocity profile of normal fluid in thermal counterflow, *Phys. Rev. Lett.* **120**, 155301 (2018).
20. D. J. Melotte and C. F. Barenghi, Transition to normal fluid turbulence in helium ii, *Phys. Rev. Lett.* **80**, 4181 (1998).
21. W. Guo, S. B. Cahn, J. A. Nikkel, W. F. Vinen, and D. N. McKinsey, Visualization study of counterflow in superfluid helium-4 using metastable helium molecules, *Phys. Rev. Lett.* **105**, 045301 (2010).
22. D. Kivotides, C. F. Barenghi, and D. C. Samuels, Triple vortex ring structure in superfluid helium ii, *Science* **290**, 777 (2000).
23. L. Galantucci, A. Baggaley, C. Barenghi, and G. Krstulovic, Quantum turbulence in superfluid helium: a self-consistent approach, *Eur. Phys. J. Plus* **135**, 547 (2020).
24. K. W. Schwarz, Three-dimensional vortex dynamics in superfluid He4, *Phys. Rev. B* **38**, 2398 (1988).
25. L. Galantucci, G. Krstulovic, and C. Barenghi, Friction-enhanced lifetime of bundled quantum vortices, *Phys. Rev. Fluids* **8**, 014702 (2023).
26. S. Inui and M. Tsubota, Coupled dynamics of quantized vortices and normal fluid in superfluid He4 based on the lattice boltzmann method, *Phys. Rev. B* **104**, 214503 (2021).
27. B. Mastracci, S. Bao, W. Guo, and W. F. Vinen, Particle tracking velocimetry applied to thermal counterflow in superfluid He4: Motion of the normal fluid at small heat fluxes, *Phys. Rev. Fluids* **4**, 083305 (2019).
28. B. Mastracci and W. Guo, Exploration of thermal counterflow in he II using particle tracking velocimetry, *Phys. Rev. Fluids* **3**, 063304 (2018).
29. N. Mordant, E. Leveque, and J. Pinton, Experimental and numerical study of the lagrangian dynamics of high reynolds turbulence, *New J. Phys.* **6**, 116 (2004).
30. C. Barenghi and D. Samuels, Scaling laws of vortex reconnections, *J. Low Temp. Phys.* **136**, 281 (2004).
31. H. Lamb, *Hydrodynamics*, Cambridge University Press , 1 (1932).
32. P. Švančara, D. Duda, P. Hrubcová, M. Rotter, L. Skrbek, M. La Mantia, E. Durozoy, P. Diribarne, B. Rousset, M. Bourgoin, *et al.*, Ubiquity of particle-vortex interactions in turbulent counterflow of superfluid helium, *J. Fluid Mech.* **911**, A8 (2021).
33. S. Yui, Y. Tang, W. Guo, H. Kobayashi, and M. Tsubota, Universal anomalous diffusion of quantized vortices in ultraquantum turbulence, *Phys. Rev. Lett.* **129**, 025301 (2022).
34. K. W. Schwarz, Turbulence in superfluid helium: steady homogenous counterflow, *Phys. Rev. B* **18**, 245 (1978).
35. D. D. Awschalom, F. P. Milliken, and K. W. Schwarz, Properties of superfluid turbulence in a large channel, *Phys. Rev. Lett.* **53**, 1372 (1984).
36. A. W. Baggaley and C. F. Barenghi, Tree method for quantum vortex dynamics, *J. Low Temp. Phys.* **166**, 3 (2012).

Methods

The FOUCAULT model. Our model considers the the superfluid as a collection \mathcal{L} of vortex lines that advect each other following Biot-Savart integrals. Vortex lines are parametrised employing arclength ξ and time t , *i.e.* the position of the vortex filaments is given by $\mathbf{s}(\xi, t)$. Regularisation of the integrals and reconnections are built following the Schwarz's vortex filament model²⁴. The vortex lines interact with the normal fluid through mutual friction coefficients β and β' as follows

$$\mathbf{v}_L = \dot{\mathbf{s}}(\xi, t) = \frac{\partial \mathbf{s}}{\partial t} = \mathbf{v}_{s\perp} + \beta \mathbf{s}' \times \mathbf{v}_{ns} - \beta' \mathbf{s}' \times (\mathbf{s}' \times \mathbf{v}_{ns}), \quad (1)$$

where $\mathbf{s}' = \partial \mathbf{s} / \partial \xi$ is the unit tangent vector, the subscript ' \perp ' indicates the component of the superfluid velocity lying on a plane orthogonal to \mathbf{s}' and $\mathbf{v}_{ns} = \mathbf{v}_n - \mathbf{v}_s$ at \mathbf{s} , with \mathbf{v}_s the superfluid velocity given by the Biot-Savart integral

$$\mathbf{v}_s(\mathbf{s}, t) = \bar{\mathbf{v}}_s + \frac{\kappa}{4\pi} \oint_{\mathcal{L}} \frac{\mathbf{s}'(\xi, t) \times (\mathbf{s} - \mathbf{s}(\xi, t))}{|\mathbf{s} - \mathbf{s}(\xi, t)|^3} d\xi. \quad (2)$$

In turn, the normal fluid satisfies the incompressible Navier-Stokes equations

$$\frac{\partial \mathbf{v}_n}{\partial t} + (\mathbf{v}_n \cdot \nabla) \mathbf{v}_n = -\frac{1}{\rho} \nabla p_n + \nu_n \nabla^2 \mathbf{v}_n + \frac{\mathbf{F}_{ns}}{\rho_n} \quad (3)$$

$$\mathbf{F}_{ns} = \oint_{\mathcal{L}} \mathbf{f}_{ns}(\mathbf{s}) \delta(\mathbf{x} - \mathbf{s}) d\xi, \quad \nabla \cdot \mathbf{v}_n = 0. \quad (4)$$

where \mathbf{F}_{ns} is mutual friction force per unit volume responsible for the retroaction of quantum vortices on \mathbf{v}_n , and

$$\mathbf{f}_{ns}(\mathbf{s}) = -D \mathbf{s}' \times [\mathbf{s}' \times (\dot{\mathbf{s}} - \mathbf{v}_n(\mathbf{s}))] - \rho_n \kappa \mathbf{s}' \times (\dot{\mathbf{s}} - \mathbf{v}_n(\mathbf{s})) \quad (5)$$

its local density, where D is a friction coefficient²³. The second term in equation 5 is the Iordanskii force: this term is responsible for the misalignment of the direction of the relative velocity between the vortex and the normal fluid (indicated by the ruler in Fig. 3 (left)) and the axis of the wake. The total density of liquid helium is $\rho = \rho_n + \rho_s$, with ρ_n and ρ_s are respectively the normal fluid and

superfluid densities. Finally, p_n is the effective pressure, and ν_n the kinematic viscosity of the normal fluid. The mean normal fluid velocity $\bar{\mathbf{v}}_n$ is directly imposed during the evolution.

A complete description of the Fully cOUpled loCAL model of sUperfLuid Turbulence (FOUCAULT), including its numerical implementation, can be found in²³.

Numerical details. The Navier-Stokes equations are solved in a periodic domain using a standard pseudo-spectral code. In all simulations we use a grid of 512^3 grid points. The vorte filament model is evolved using a Tree-Algorithm method³⁶ that allows for an important speed up of the Biot-Savart computations. The number of discretisation points used to represent the vortex lines is adapted during the simulations, and fluctuates in the steady state around 700 and 10^4 for $v_{ns}^{(1)}$ and $v_{ns}^{(2)}$, respectively.

Data availability

Data is availability upon request.

Acknowledgements

We acknowledge discussions with Profs Marco La Mantia, Mathieu Gibert and Wei Guo. G.K. acknowledges support of Agence Nationale de la Recherche through the project QuantumVIW ANR-23-CE30-0024-02.

Author contributions

L.G ran the simulations and processed the data. All authors contributed to writing the paper.

Competing interests

The authors declare no competing interests.

Supplementary Information

Single vortex wake at $v_{ns} = v_{ns}^{(2)} = 0.94\text{cm/s}$

The pattern of the normal fluid past a single vortex at counterflow velocity $v_{ns} = v_{ns}^{(1)} = 0.27\text{ cm/s}$ was shown in Fig. 3 of the main text. For completeness, Fig. 5 displays the wake generated by a single, straight superfluid vortex oriented in the positive y -direction in the presence of counterflow in the z -direction at counterflow velocity $v_{ns} = v_{ns}^{(2)} = 0.94\text{cm/s}$ at $t \approx \tau_r/10$. In the left panel, we report the relative normal fluid streamwise velocity fluctuations $\Delta v_n^z = \delta v_n^z / \bar{v}_n^z = (v_n^z(x, z) - \bar{v}_n^z) / \bar{v}_n^z$ vs x and z at fixed y_0 . In the centre (right) panel we report the PDFs of the streamwise (spanwise) normal fluid velocity fluctuations δv_n^z (δv_n^x). With respect to the spanwise (x) fluctuations (Fig. 5, right), the PDF has been computed taking also into account the fluctuations generated by a vortex oriented in the negative y -direction (this is not necessary for the streamwise component as in this circumstance the fluctuations generated coincide).

Calculation of wake size in the single vortex simulation

For both counterflow velocities $v_{ns}^{(1)}$ and $v_{ns}^{(2)}$ we compute the size of the wake at $t \approx \tau_r/10$, employing the two-dimensional normal fluid velocity field resulting from the motion of a single, straight superfluid vortex in presence of a counterflow. The corresponding relative streamwise velocity fluctuations $(v_n^z(x, z) - \bar{v}_n^z) / \bar{v}_n^z$ have been reported in Fig. 3 (left) in the main text and Fig. 5 (left) in the Supplementary Information for $v_{ns}^{(1)}$ and $v_{ns}^{(2)}$, respectively. The size of the wake, w , is defined as follows:

$$w = \sqrt{\frac{\int_{\mathcal{S}} |\mathbf{x} - \mathbf{s}_0|^2 |\delta \tilde{\mathbf{v}}_n|^2 dx dz}{\int_{\mathcal{S}} |\delta \tilde{\mathbf{v}}_n|^2 dx dz}}, \quad (6)$$

where \mathcal{S} is the x - z two-dimensional domain orthogonal to the superfluid vortex at fixed y_0 (i.e. the domain reported in Fig. 3 (left) in the main text and Fig. 5 (left) in the Supplementary Information); $\mathbf{x} = (x, z)$ is the general position vector; \mathbf{s}_0 is the intersection of the vortex with \mathcal{S} at $t \approx \tau_r/10$; $\delta \tilde{\mathbf{v}}_n = (v_n^x, v_n^y, v_n^z - \bar{v}_n^z)$.

Oseen solution

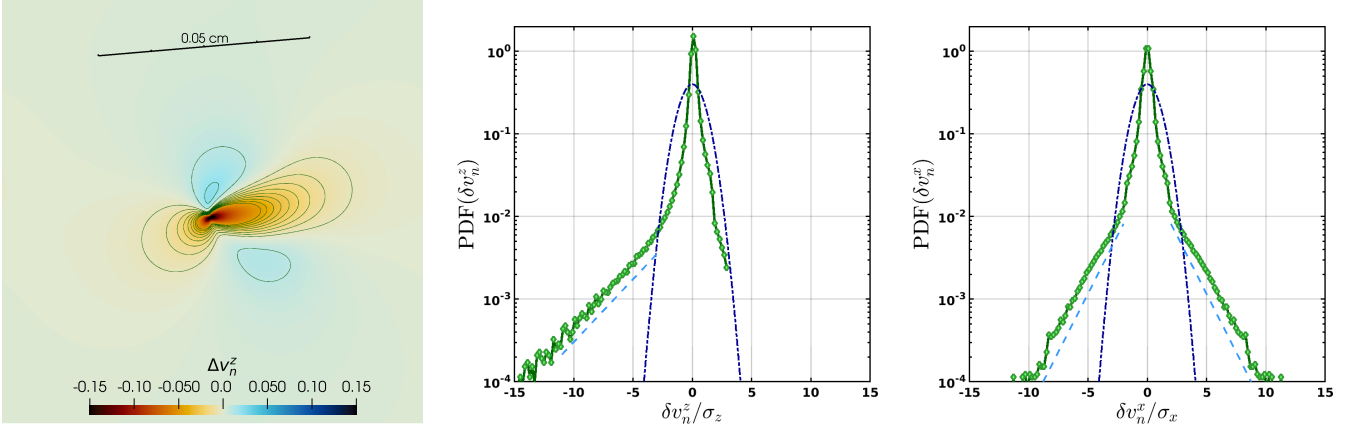


Fig. 5 Single vortex wake. Temperature $T = 1.5$ K and $v_{ns}^{(2)} = 0.94$ cm/s. Left column: relative normal fluid streamwise velocity fluctuations $\Delta v_n^z = \delta v_n^z / \bar{v}_n^z = (v_n^z(x, z) - \bar{v}_n^z) / \bar{v}_n^z$ vs x and z at fixed y_0 . The ruler indicates the direction of the relative velocity of the single vortex line with respect to the normal fluid. Centre column: PDF(δv_n^z) vs $\delta v_n^z / \sigma_z$, where $\delta v_n^z = v_n^z - \bar{v}_n^z$ and σ_z is the standard deviation. Right column: PDF(δv_n^x) vs $\delta v_n^x / \sigma_x$, where $\delta v_n^x = v_n^x$ ($\bar{v}_n^x = 0$) and σ_x is the standard deviation. Gaussian distributions are shown in dot-dashed dark blue line for reference. The dashed cyan lines are exponential functions to guide the eye.

In two-dimensions, the Stokes equation describing the steady flow of a viscous fluid past a circle at low Reynolds number has no solution: it is impossible to enforce simultaneously no-slip boundary condition on the circle the condition of and uniform flow at infinity (Stokes' paradox). In order to determine the flow of the fluid, it is necessary to employ Oseen's equation³¹ including a linearised convective term. With reference to Fig. 6, the velocity of the viscous fluid \mathbf{V} can be expressed in terms of the velocity of the fluid at infinity \mathbf{U} and a perturbation \mathbf{v} , as follows $\mathbf{V} = \mathbf{U} + \mathbf{v}$, where $\mathbf{U} = U\hat{\mathbf{k}}$, $\hat{\mathbf{k}}$ being the unit vector in the z (horizontal) direction (x is the vertical direction). At large distances $r \gg a_0$, (the distances we are interested in, $\mathbf{V} \approx \mathbf{U}$ (or, equivalently, $v \ll U$) and hence the convective term may be approximated as follows, $(\mathbf{V} \cdot \nabla)\mathbf{V} \approx U \frac{\partial}{\partial z} \mathbf{v}$ leading to the Oseen equation for the perturbation \mathbf{v} :

$$U \frac{\partial}{\partial z} \mathbf{v} = -\frac{1}{\rho} \nabla p + \nu \nabla^2 \mathbf{v}. \quad (7)$$

The non-dimensional far field solution of equation (7), *i.e.* the solution for $r \gg a_0/Re$, is in polar coordinates³¹

$$\begin{aligned} v_r' &= \frac{C_0}{2} \sqrt{\frac{\pi}{\tilde{r}}} (1 + \cos \theta) e^{-\frac{\tilde{r}}{2}(1 - \cos \theta)} - \frac{C_0}{\tilde{r}}, \\ v_\theta' &= -\frac{C_0}{2} \sqrt{\frac{\pi}{\tilde{r}}} \sin \theta e^{-\frac{\tilde{r}}{2}(1 - \cos \theta)}, \end{aligned} \quad (8)$$

where $\tilde{r} = r \frac{Re}{a_0}$ is the Oseen non-dimensional variable (the far field corresponds to $\tilde{r} \gg 1$),

$$C_0 = -\frac{2}{0.5 - \gamma - \log(\epsilon/2)}, \quad (9)$$

$\gamma = 0.5772$ is the Euler-Mascheroni constant and $v' = v/U$. The resulting far-field vorticity ω is given by the following expression

$$\omega = \frac{C_0 Re}{2} \sin \theta e^{-\frac{\tilde{r}}{2}(1 - \cos \theta)} \sqrt{\frac{\pi}{\tilde{r}}}, \quad (10)$$

whose spatial dependence is reported in Fig. 7. It is important to note the upstream/downstream asymmetry.

The far field solution of Oseen's equation (8) can be employed to determine the spatial dependence of the flow in the far wake, *i.e.* for $\tilde{r} \gg 1$ and $\theta \ll 1$. In this region the flow is described by the following expressions

$$\begin{aligned} v_r' &= C_0 \sqrt{\frac{\pi}{\tilde{r}}} e^{-\frac{\tilde{r}\theta^2}{4}} - \frac{C_0}{\tilde{r}}, \\ v_\theta' &= -\frac{C_0}{2} \sqrt{\frac{\pi}{\tilde{r}}} \theta e^{-\frac{\tilde{r}\theta^2}{4}}, \end{aligned} \quad (11)$$

whose streamwise component $v'^z = (V^z - U)/U$ is reported in Fig. 8. The iso-lines in Fig. 8 are drawn at the same values of the relative magnitude of streamwise velocity fluctuations employed in Fig. 3. If we compare the linear sizes of the wakes (*e.g.* the linear size of the region where $v'^z < -0.05$) we find very good agreement between the analytical solution of Oseen's equation and our numerical results. Furthermore, if we compute the PDFs of the streamwise and spanwise velocity fluctuations, v^z and v^x , respectively reported in Fig. 9 (left) and (right), in the far wake (for $\tilde{r} > 10$ and $\theta \ll 10^\circ$), we recover the same characteristics observed for the normal fluid in our counterflow turbulence simulations and in the analysis of the single vortex wake: the PDFs are skewed and/or with exponential tails. This similarity supports our conclusion that the normal fluid in a turbulent helium counterflow

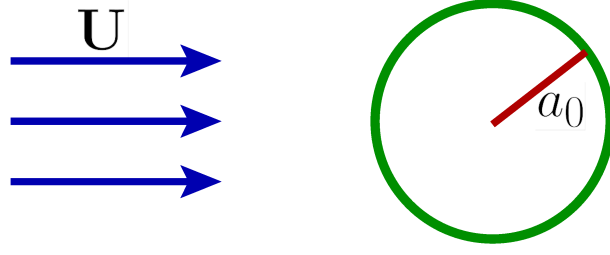


Fig. 6 Schematic rendering of the two-dimensional flow past a circle.

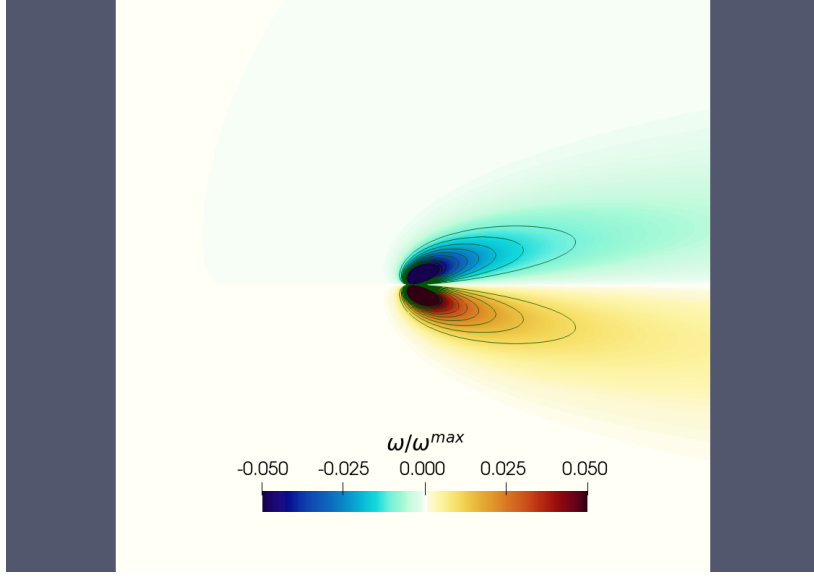


Fig. 7 Far field Oseen solution: vorticity field normalised by its maximum value ω/ω_{max} . The size of the domain is 0.1 cm.

is the superposition of a uniform background flow generated by the heater and flow disturbances (consisting of small vortex dipoles and large almost parabolic wakes) generated by the vortices via the friction force.

Skewness of vortex velocity v_L

Consider equation (1). For $T \geq 1.5\text{K}$ (the temperature range where the $\rho_n/\rho > 0.1$) we have $|\beta'| > \beta > 0$, hence the streamwise vortex velocity v_L^z can be written as follows:

$$\begin{aligned} v_L^z(\mathbf{s}) &= (1 - |\beta'|)(\bar{v}_s^z + v_{BS}^z(\mathbf{s})) + |\beta'|v_n^z(\mathbf{s}) \\ &= \varepsilon_1(\bar{v}_s^z + v_{BS}^z(\mathbf{s})) + \varepsilon_2v_n^z(\mathbf{s}) , \end{aligned} \quad (12)$$

where $v_{BS}^z(\mathbf{s})$ is the streamwise component of the Biot-Savart integral in equation (2), $\varepsilon_1 = 1 - |\beta'| = 0.88$, $\varepsilon_2 = |\beta'| = 0.12$, $\varepsilon_1 + \varepsilon_2 = 1$, ε_1 and ε_2 depend on temperature T and Reynolds number and as temperature

increases $\varepsilon_1 \rightarrow 0$ and $\varepsilon_2 \rightarrow 1$. Values of ε_1 and ε_2 reported are evaluated at $T = 1.5\text{K}^{23}$, and the velocities v_{BS}^z and v_n^z are evaluated on the vortex positions \mathbf{s} .

Equation (12) implies that, in the first approximation, the streamwise vortex velocity fluctuation δv_L^z has the following expression:

$$\delta v_L^z(\mathbf{s}) = \varepsilon_1\delta v_{BS}^z(\mathbf{s}) + \varepsilon_2\delta v_n^z(\mathbf{s}) \quad (13)$$

To quantify the asymmetry of the PDF of δv_L^z (reported in Fig. 4 and echoing the experimental non symmetric distribution of the streamwise velocity of particles likely trapped on vortices³²), the relevant quantity to compute is the skewness of v_L^z defined as $\mathcal{S}(v_L^z) = \overline{[\delta v_L^z(\mathbf{s})]^3}$ which, following equation (13), depends on $\mathcal{S}(v_{BS}^z)$, $\mathcal{S}(v_n^z)$ and other velocity cross correlation terms. For $v_{ns} = v_{ns}^{(2)} = 0.94 \text{ cm/s}$ (as experiments in Ref.³² are performed at large v_{ns}) we obtain the following values for the skewnesses (in non-dimensional units scaled with unit of length $\lambda = 1.59 \times 10^{-2} \text{ cm}$ and unit of time $\tau = 1.22 \times 10^{-2} \text{ s}$): $\mathcal{S}(v_L^z) = -2.3 \times 10^{-4}$, $\mathcal{S}(v_{BS}^z) = -1.8 \times 10^{-4}$ and $\mathcal{S}(v_n^z) = -8 \times 10^{-4}$. Hence, the skewness of v_{BS}^z does not fully account for the skewness of v_L^z , implying that the skewness of v_n^z arising from the existence of the wakes, contributes to $\mathcal{S}(v_L^z)$ and

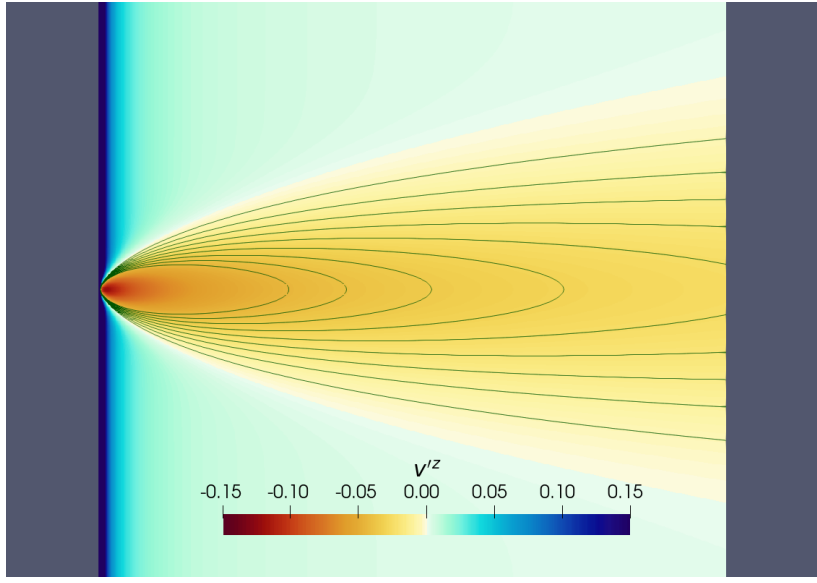


Fig. 8 Far Wake Oseen solution: relative magnitude of the streamwise velocity fluctuations $v'^z = v^z/U = (V^z - U)/U$. The size of the domain is 0.1 cm. Iso-lines are drawn at the same values as in Figs. 3 and 5.

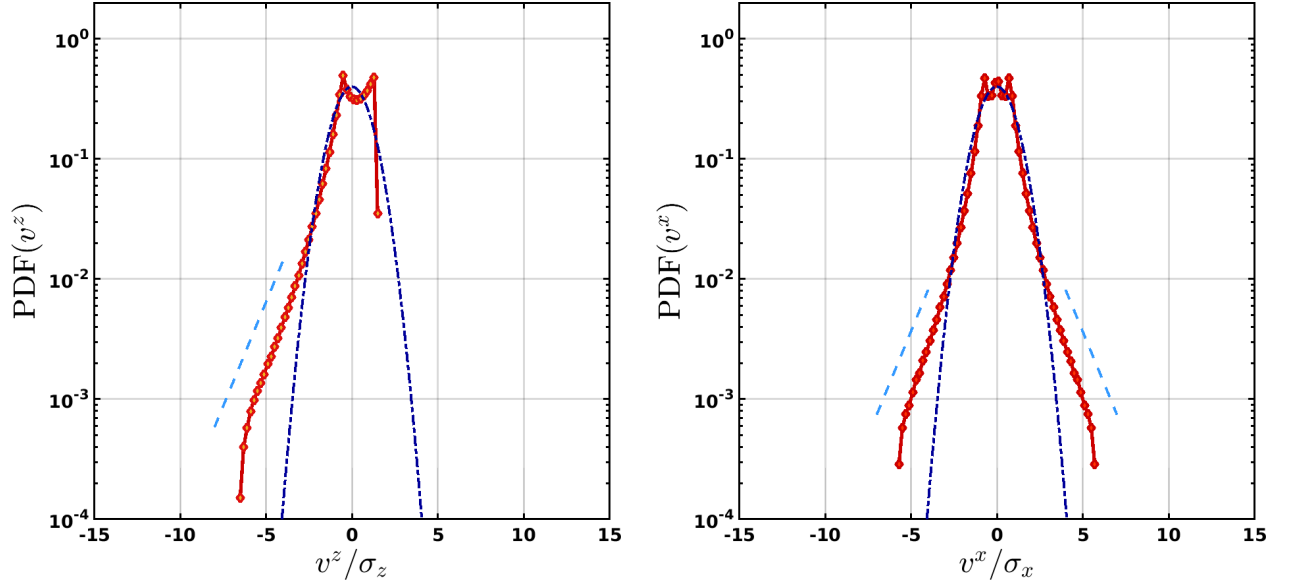


Fig. 9 Far wake Oseen solution: Left: $\text{PDF}(v^z)$ vs v^z/σ_z , where v^z is the streamwise velocity fluctuation of the solution of Oseen's equation in the far wake region and σ_z is the standard deviation. Right: $\text{PDF}(v^x)$ vs v^x/σ_x , where v^x is the spanwise velocity fluctuation of the solution of Oseen's equation in the far wake region and σ_x is the standard deviation. Gaussian distributions are showed in dot-dashed dark blue line for reference. The dashed cyan lines are exponential functions to guide the eye.

hence to the non symmetrical character of the statistical distributions of the velocity of inertial particles observed in

experiments³². As ε_2 increases for increasing temperature, the impact of the wakes on the experimental particle velocity statistics is likely to increase with temperature.